New Journal of Physics
The open-access journal for physics

The Shapiro effect in atomchip-based bosonic Josephson junctions

Julian Grond[1,2,3,4,5], Thomas Betz[1], Ulrich Hohenester[3], Norbert J Mauser[2], Jörg Schmiedmayer[1] and Thorsten Schumm[1,2]

[1] Vienna Center for Quantum Science and Technology (VCQ), Atominstitut, TU-Wien, Stadionalle 2, 1020 Vienna, Austria
[2] Wolfgang Pauli Institut, c/o Fak. Mathematik, Universität Wien, Nordbergstrasse 15, 1090 Vienna, Austria
[3] Institut für Physik, Karl-Franzens-Universität Graz, Universitätsplatz 5, 8010 Graz, Austria
[4] Theoretische Chemie, Physikalisch-Chemisches Institut, Universität Heidelberg, Im Neuenheimer Feld 229, 69120 Heidelberg, Germany
E-mail: julian.grond@pci.uni-heidelberg.de

New Journal of Physics **13** (2011) 065026 (15pp)
Received 4 February 2011
Published 28 June 2011
Online at http://www.njp.org/
doi:10.1088/1367-2630/13/6/065026

Abstract. We analyze the emergence of Shapiro resonances in tunnel-coupled Bose–Einstein condensates, realizing a bosonic Josephson junction. Our analysis is based on an experimentally relevant implementation using magnetic double-well potentials on an atomchip. In this configuration, the potential bias (implementing the junction voltage) and the potential barrier (realizing the Josephson link) are intrinsically coupled. We show that the dynamically driven system exhibits significantly *enhanced Shapiro resonances* which will facilitate experimental observation. To describe the system's response to the dynamic drive, we compare a single-mode Gross–Pitaevskii (GP) description, an improved two-mode (TM) model and the self-consistent multi-configurational time-dependent Hartree equations for bosons (MCTDHB) method. We show that in the case of significant atom–atom interactions, the spatial dynamics of the involved modes has to be taken into account and only the MCTDHB method allows reliable predictions.

[5] Author to whom any correspondence should be addressed.

Contents

1. Introduction

Coherent tunneling dynamics of macroscopic many-body quantum states through a classically forbidden barrier is one of the most striking manifestations of quantum physics. In the presence of an external drive, such systems exhibit the *Shapiro effect*, also known as *photon-assisted tunneling* [1, 2]. Shapiro resonances have been studied extensively in the context of solid-state superconducting Josephson junctions, where a resonant modulation of the energy bias leads to a dc current across the junction [1, 3]. Such resonances can be used to exactly quantify an applied dc potential difference across the junction and are nowadays used to implement a voltage standard.

A similar effect occurs in tunnel-coupled Bose–Einstein condensates (BECs) in double-well potentials, where a resonant modulation of an additional linear potential ramp induces a condensate oscillation between both wells [2]. This could have important applications, such as the accurate measurement of the chemical potential difference across the tunnel barrier [4], or of a potential difference between both wells, which might allow gravity measurements on very small spatial scales or close to surfaces [5]. In contrast to superconducting systems, the dynamics of the *bosonic Josephson junction* is strongly influenced by atom–atom interactions [6], leading to several novel effects that will be the subject of this paper. In addition, atomchips provide highly tuneable tunnel coupling and interaction parameters [7] and allow for a direct access to the canonical observables number and phase, instead of indirect values such as current and flux. Furthermore, they allow for the study of π-phase modes, macroscopic quantum self-trapping [6, 8], bistability and critical behavior [9].

In recent years, much effort has been devoted to the theoretical and experimental study of the tunneling dynamics of undriven and driven BECs [10]. The direct analogy to the superconducting Josephson junction has been realized in an all-optical double-well potential. Here the influence of atom–atom interactions has been evidenced, leading to new dynamical modes [11] and sub-Poissonian number statistics [12]. In optical lattice experiments, arrays of bosonic Josephson junctions have been realized [13]. Shaking of the optical lattice allowed the

control of the effective tunnel coupling [14], the superfluid-to-Mott-insulator transition [15] and dynamical localization [16].

In this work, we analyze the Shapiro effect for magnetic double-well potentials on atomchips in view of a recent experimental realization of a bosonic Josephson junction [17]. We focus on the experimentally relevant situation where a modulation of the energy bias between the left and right wells is accompanied by a concurrent modulation of the tunnel coupling. As we show, this leads to a significant enhancement of the Shapiro resonances compared to the conventional driving [2], which will facilitate experimental observation.

In solid-state physics, Shapiro resonances are conveniently analyzed using a two-mode (TM) model [1]. For driven ultracold atom systems, it is important to additionally take into account the spatial degrees of freedom, as excitations might be induced by the external drive, which can have a strong influence on the tunneling dynamics. Within the BEC community, one usually employs the Gross–Pitaevskii (GP) equation in order to describe the spatial dynamics of the condensate [18]. It is based on the assumption of a single condensate wave function, which is coherent over both wells. This is obviously not the case for bosonic Josephson junctions and thus provides an insufficient description of the problem under study. To bridge the description schemes of the solid-state and cold atom communities, in this work we additionally employ the *multi-configurational time-dependent Hartree equations for bosons* (MCTDHB) method [19, 20], which is a self-consistent approach taking into account the full dynamics of the system. In principle, it allows for a numerically exact solution of the many-body Schrödinger equation and can thus be used as a reference calculation for comparison with simpler models.

Previously, the MCTDHB method applied to bosonic Josephson junctions allowed the discovery of dynamics very different from those predicted by the GP equation and the TM model, such as an *inverse* splitting regime [21], the decay of macroscopic quantum self-trapping [22], fast loss of coherence in low-dimensional attractive solitons [23] and violation of time-reversal symmetry when switching interactions from repulsive to attractive in bosonic Josephson junctions [24]. In this work, we also study the case when for typical interaction strengths, the Shapiro resonance structure predicted from MCTDHB appreciably differs from simpler models.

This paper is organized as follows. We start with the physical system and its dynamic description in section 2. In section 2.1, we introduce the realization of the double-well potential and how we implement the driving. In section 2.2, we outline the three models which will be used and compared in this work: the GP equation, the TM model and MCTDHB. In section 3, the non-interacting driven system is discussed, and results that demonstrate *enhanced Shapiro resonances* are shown. It includes a short discussion of how to choose experimental parameters in order to observe the effect. Results for the case with interactions are presented in section 4. First we show how the resonances shift due to interactions in section 4.1. A discussion of the different dynamical models, as well as the damping of the oscillations in the number imbalance, is finally presented in section 4.2.

2. Physical system

2.1. Double-well potential

The following analysis is motivated by a recent experimental realization of a bosonic Josephson junction on an atomchip [17]. A symmetric double-well potential is generated by a combination

of static and oscillating magnetic near fields, making use of dressed adiabatic states [25–27][6]. The system consists of two elongated traps with strong atomic confinement ($\omega_\perp \sim 2\pi \times 2\,\mathrm{kHz}$) in the x- and y (transverse)-directions, and a very weak confinement along the z (longitudinal)-direction with $\omega_{x,y}/\omega_z \sim 100$. Tunneling dynamics takes place along the coupling direction x, which connects the two potential minima of the double well. The system is assumed to remain in the (many-particle) ground state in the two orthogonal directions y and z which do not contribute to the dynamics. The distance d between the double-well minima and the height of the tunnel barrier are adjusted by controlling the amplitude of the oscillating field component, which is in the radio frequency (RF) range. This RF amplitude represents the dynamical control parameter used to drive the Shapiro resonances. To implement a potential difference ('voltage') between both wells, the double well can be tilted in space (making use of gravity) [5, 25]. Further possibilities are a spatial inhomogeneity in the amplitude of the RF field, dc electric near fields [28] or local optical dipole potentials [11, 29].

The resulting potential is given by equation (10) of [26] and can be approximately described by a symmetric fourth-order polynom $V_\lambda(x)$ for the double well with an additional linear gradient g that implements the tilt:

$$V_{\lambda,g}(x) = V_\lambda(x) + g \cdot x, \quad \text{with } V_\lambda(x) = c(\lambda) \cdot (x^2 - (d(\lambda)/2)^2)^2. \tag{1}$$

Note that the control parameter $\lambda(t)$ (RF amplitude) affects both the separation of the double-well minima and the steepness of the confinement. By construction, a larger separation coincides with a higher potential barrier, both reducing coupling. This makes $\lambda(t)$ the most sensitive parameter in the system.

The most straightforward implementation of a Shapiro experiment would be to dynamically modulate the potential gradient g. However, in a purely magnetic implementation of the double well as in [17], this would also result in a significant spatial displacement of the trap minima, which might lead to excitations and uncontrolled dynamics. We therefore focus the analysis on the effects of a periodic modulation of the RF amplitude (splitting parameter $\lambda(t)$) keeping g fixed. This results in double-well minima moving along a potential slope as indicated in figure 1 (upper right inset). As we will show, modulating both the tunnel coupling and the potential difference leads to a significant enhancement of the observed Shapiro resonances.

2.2. Model

2.2.1. Many-body Hamiltonian. In this work, we consider the dynamics in the splitting direction x and neglect any dynamics in the other directions y and z. The dynamics of the atoms in the double well is then governed by the many-body Hamiltonian [18, 30]

$$\hat{H}(t) = \int \left[\hat{\Psi}^\dagger(x) \hat{h}^\lambda(x) \hat{\Psi}(x) + \frac{\hbar U_0}{2} \hat{\Psi}^\dagger(x) \hat{\Psi}^\dagger(x) \hat{\Psi}(x) \hat{\Psi}(x) \right] \mathrm{d}x, \tag{2}$$

where $\hat{\Psi}(x)$ is the bosonic field operator, and $\hat{h}^\lambda(x) = -\frac{\hbar^2}{2m}\nabla^2 + V_{\lambda,g}(x)$ is the *bare* Hamiltonian. U_0 is the effective one-dimensional (1D) interaction strength, obtained by integrating out the other spatial directions for the ground state [31]. The 1D approximation is reasonable since typically the dynamics in the other directions decouples to a good extent whenever the 3D potential factorizes, i.e. $V(\mathbf{r}) = V_x(x) + V_y(y) + V_z(z)$.

[6] The considerations made in this work are equally valid for double-well systems based on solely static magnetic fields or on optical dipole potentials.

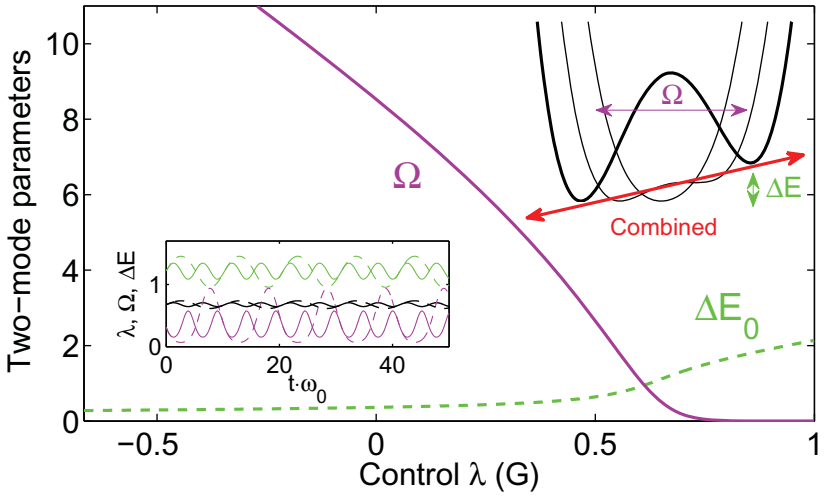

Figure 1. Ω and ΔE versus λ, calculated using eigenstates of the Schrödinger equation. Upper right inset: driving geometry. Lower left inset: when the splitting parameter λ (black lines) is driven periodically, both Ω (violet lines) and ΔE (green lines) oscillate (in units of ω_0 as defined in section 4.1). Solid line: first resonance $n = 1$ for the non-interacting system, with parameters as in the text. Dashed line: second resonance $n = 2$ (with larger amplitude).

Direct solution of the equations of motion following from this Hamiltonian is not possible for more than a few atoms, and thus we have to use approximation schemes. In this paper, we will employ and compare several types of approximations and solution schemes that we will introduce in the following. They can be considered as different ways of restricting the field operator $\hat{\Psi}(x)$ to a small number of modes.

2.2.2. The Gross–Pitaevskii (GP) equation. The mean-field dynamics [18] is obtained by restricting the field operator to a single mode function, $\hat{\Psi}(x) = \hat{a}_0\phi_0(x)$. The Heisenberg equation of motion for $\hat{\Psi}(x)$, obtained from equation (2), yields the GP equation

$$\mathrm{i}\hbar\dot{\phi}_0(x,t) = \left(\hat{h}^{\lambda}(x) + U_0(N-1)|\phi_0(x,t)|^2\right)\phi_0(x,t). \tag{3}$$

For a BEC in a double well, the GP wave function can be written as $\phi_0(x) = [\phi_{\mathrm{L}}(x) + \phi_{\mathrm{R}}(x)]/\sqrt{2}$, where $\phi_{\mathrm{L}}(x)$ $[\phi_{\mathrm{R}}(x)]$ is localized in the left (right) well. The probability for finding n out of N atoms in the left well can be calculated as

$$\begin{aligned} P_n &= \int_{-\infty}^{0} \mathrm{d}x_1 \ldots \mathrm{d}x_n \int_{0}^{-\infty} \mathrm{d}x_{n+1} \ldots \mathrm{d}x_N \, \mathcal{S}\Pi_{i=1}^{N}[\phi_L(x_i) + \phi_R(x_i)]/\sqrt{2} \\ &= \frac{1}{2^{N/2}}\binom{N}{n}, \end{aligned} \tag{4}$$

where $\mathcal{S}$ is the symmetrization operator. The GP equation assumes thus that the number distribution between the left and right localized condensates has binomial number fluctuations $\sqrt{N}$ (perfectly 'coherent state' [32]). Since for the initial state we consider in this work always a condensate localized in one well, the GP equation will properly describe the short time dynamics. At longer times, however, a single-mode description will not be valid anymore.

2.2.3. Two-mode (TM) model. In a double well, it is more natural to use a basis that comprises two modes instead of one: $\hat{\Psi}^{\lambda}(x) = \hat{a}_{\mathrm{L}}\phi_{\mathrm{L}}^{\lambda}(x) + \hat{a}_{\mathrm{R}}\phi_{\mathrm{R}}^{\lambda}(x)$. Here, the localized mode functions $\phi_{\mathrm{L}}^{\lambda}(x)$ and $\phi_{\mathrm{R}}^{\lambda}(x)$ depend on the control parameter λ. $\hat{a}_{\mathrm{L}}$ ($\hat{a}_{\mathrm{L}}^{\dagger}$) annihilates (creates) an atom in the left well, and similar $\hat{a}_{\mathrm{R}}$ ($\hat{a}_{\mathrm{R}}^{\dagger}$).

There exist several schemes for the choice of the modes $\phi_{\mathrm{L}}^{\lambda}(x)$ and $\phi_{\mathrm{R}}^{\lambda}(x)$. The simplest one uses superpositions of the two lowest-lying eigenstates $\phi_{\mathrm{g}}^{\lambda}(x)$ and $\phi_{\mathrm{e}}^{\lambda}(x)$ of the single-particle Schrödinger equation of the symmetric potential $V_{\lambda}(x)$, which have gerade and ungerade symmetry: $\phi_{\mathrm{L,R}}^{\lambda}(x) = [\phi_{\mathrm{g}}^{\lambda}(x) \pm \phi_{\mathrm{e}}^{\lambda}(x)]/\sqrt{2}$ [33]. The Hamiltonian reads in terms of pseudo-spin operators:

$$H = -\hbar\Omega(t)\hat{J}_x + \hbar\Delta E(t)\hat{J}_z + 2\hbar\kappa(t)\hat{J}_z^2. \tag{5}$$

Hereby, $\hat{J}_z = \frac{1}{2}(\hat{a}_{\mathrm{L}}^{\dagger}\hat{a}_{\mathrm{L}} - \hat{a}_{\mathrm{R}}^{\dagger}\hat{a}_{\mathrm{R}})$ measures the atom number difference between left and right wells, and $\hat{J}_x = \frac{1}{2}(\hat{a}_{\mathrm{L}}^{\dagger}\hat{a}_{\mathrm{R}} + \hat{a}_{\mathrm{R}}^{\dagger}\hat{a}_{\mathrm{L}})$ promotes an atom from the left to the right well and vice versa. Equation (5) depends on the generic parameters $\Omega(t)$, $\Delta E(t)$ and $\kappa(t)$, which denote the tunnel coupling, energy bias and nonlinear interaction energy, respectively. They are given as

$$\begin{aligned}
\Omega(t) &= -\frac{1}{\hbar}\int \mathrm{d}x\,\phi_{\mathrm{L}}^{*,\lambda}(x)\hat{h}^{\lambda}(x)\phi_{\mathrm{R}}^{\lambda}(x) + \mathrm{h.c.},\\
\Delta E(t) &= \frac{1}{\hbar}\int \mathrm{d}x\,\phi_{\mathrm{L}}^{*,\lambda}(x)\hat{h}^{\lambda}(x)\phi_{\mathrm{L}}^{\lambda}(x) - \frac{1}{\hbar}\int \mathrm{d}x\,\phi_{\mathrm{R}}^{*,\lambda}(x)\hat{h}^{\lambda}(x)\phi_{\mathrm{R}}^{\lambda}(x),\\
\kappa(t) &= \frac{U_0}{2}\int \mathrm{d}x\,|\phi_{\mathrm{L}}^{\lambda}(x)|^4.
\end{aligned} \tag{6}$$

The time dependence in these parameters is due to a time-dependent control $\lambda(t)$. Tunnel coupling and energy bias between left and right condensates are shown in figure 1 over a wide range of λ from the unsplit to the split case. While the tunnel coupling decreases with increased splitting, the energy bias becomes larger. Typically, we choose a constant $\kappa \approx U_0/2$, which is a good approximation because this value depends less crucially on the shape of the modes as compared with $\Omega(t)$ and $\Delta E(t)$.

An *improved* TM model [34] can be obtained by refining the estimation of the tunnel coupling. Thus, the first and second self-consistent states of the GP equation $\phi_{\mathrm{g}}^{\mathrm{GP},\lambda}(x)$ and $\phi_{\mathrm{e}}^{\mathrm{GP},\lambda}(x)$ are used, with energies $E_{\mathrm{g}}^{\mathrm{GP},\lambda}$ and $E_{\mathrm{e}}^{\mathrm{GP},\lambda}$, respectively. The tunnel coupling of the improved model $\Omega^{(\mathrm{I})}$ is given by the energy difference $E_{\mathrm{e}}^{\mathrm{GP},\lambda}$–$E_{\mathrm{g}}^{\mathrm{GP},\lambda}$ and a shift due to interactions.[7] The parameters for the improved model are then given by

$$\Omega^{(\mathrm{I})}(t) = E_{\mathrm{e}}^{\mathrm{GP},\lambda} - E_{\mathrm{g}}^{\mathrm{GP},\lambda} - U_0 N/2\left(\int \mathrm{d}x|\phi_{\mathrm{e}}^{\mathrm{GP},\lambda}|^4 - \int \mathrm{d}x|\phi_{\mathrm{g}}^{\mathrm{GP},\lambda}|^4\right), \tag{7}$$

$$\Delta E^{(\mathrm{I})}(t) = \frac{1}{\hbar}\int \mathrm{d}x[\phi_{\mathrm{L}}^{\mathrm{GP},\lambda}]^*\hat{h}^{\lambda}\phi_{\mathrm{L}}^{\mathrm{GP},\lambda} - \frac{1}{\hbar}\int \mathrm{d}x[\phi_{\mathrm{R}}^{\mathrm{GP},\lambda}]^*\hat{h}^{\lambda}\phi_{\mathrm{R}}^{\mathrm{GP},\lambda}. \tag{8}$$

In the following, we always use the improved TM model.

[7] Other, more subtle corrections to the standard TM model (e.g. to κ), as suggested by Ananikian and Bergeman [34], will not be used here since they do not lead to significant improvements in our results.

2.2.4. TM model with self-consistent orbitals and occupations. One way to bridge the GP (spatial dynamics) and the TM (hopping) descriptions is to use two time-dependent orbitals in a self-consistent fashion. Such a scheme is provided by the MCTDHB method [19–21]. The basic idea of MCTDHB is to make an ansatz for the many-body state in terms of superpositions of symmetrized states (permanents). The number of permanents is chosen at will; in this work, we will use two for the description of a double-well system. The ansatz for the field operator then reads $\hat{\Psi}^{\lambda}(x) = \hat{a}_{\mathrm{L}}(t)\phi^{\lambda}_{\mathrm{L}}(x,t) + \hat{a}_{\mathrm{R}}(t)\phi^{\lambda}_{\mathrm{R}}(x,t)$. Based on this ansatz, an action integral is formulated and variational calculus is applied to determine the 'best-possible' shape of the orbitals at a given time. Then, the working equations for the orbitals, which enter the permanents, as well as for the coefficients of the permanents (or state vector), are derived. The equations for the orbitals are coupled, nonlinear equations, with nonlinearities depending on the one- and two-body reduced density matrices. They are coupled to the equation for the state vector, which is governed by the general many-body Hamiltonian in terms of the mode operators, with matrix elements depending again on the orbitals. The resulting self-consistent set of equations has to be solved simultaneously. MCTDHB can be considered a generalization of the GP equation, which is obtained from MCTDHB in the limiting case for $M = 1$ orbitals. Most importantly, the only approximation involved is the finite number of modes. Hence, for a large enough number of modes, the method allows, at least in principle, for a numerically exact solution of the many-body Schrödinger equation, equation (2). A detailed discussion on the working equations of MCTDHB can be found elsewhere [19, 31].

An important quantity of the MCTDHB approach is the one-body reduced density $\langle\hat{\Psi}^{\dagger}(x)\hat{\Psi}(x)\rangle$ [35], which can be diagonalized to give the natural orbitals $\phi_i(x)$ and occupations ρ_i $(i = 1, 2)$:

$$\rho(x) = \sum_{i=1}^{2} \rho_i |\phi_i(x)|^2. \tag{9}$$

Whenever one natural occupation dominates, we have a BEC [36], and whenever several eigenvalues are finite, we have an m fold fragmented BEC. In this work, we measure the degree of fragmentation by the difference in population of the natural orbitals: $(\rho_{11} - \rho_{22})/N = \pm 1$ corresponds to a single BEC, whereas $(\rho_{11} - \rho_{22})/N = 0$ corresponds to a fully fragmented system.

2.3. Observable

The Shapiro effect in a superconducting Josephson junction is related to a finite dc component of the tunnel current at the resonance frequencies. A similar effect is present in a bosonic Josephson junction. However, in typical atomchip experiments, current cannot be measured directly and furthermore the reservoirs, consisting of the atoms in the left or right well, are finite. Therefore, the 'current' changes its sign whenever one reservoir is empty and in such a manner that the atoms oscillate between both wells.

Since the initial configuration for the following investigation consists of all atoms in the lower well, i.e. $\langle\hat{J}_z(t=0)\rangle = N/2$, a Shapiro resonance can be characterized by a reduced time-averaged imbalance [2]

$$\langle\hat{J}_z\rangle_{\mathrm{T}} \equiv \frac{1}{T}\int_0^{\mathrm{T}} \mathrm{d}t\,\langle\hat{J}_z(t)\rangle, \tag{10}$$

whereby a value close to zero indicates a complete tunneling of atoms between both wells.

3. Shapiro resonances in the absence of interactions

We now discuss the emergence of Shapiro resonances in the atomchip geometry, where the double-well separation is modulated in the presence of a fixed potential gradient. We first neglect atom–atom interactions in our simulations. This system can then be well captured by the TM model.

3.1. Enhanced Shapiro effect

The time dependence of the control parameter is chosen as

$$\lambda(t) = \lambda_0 + \lambda_1 \sin(\omega t), \tag{11}$$

with driving frequency ω. In the following, we take $\lambda_0 = 0.675$, corresponding to a splitting distance of approximately $2\,\mu$m, and a gradient $g/\hbar = 2\pi \times 174.87\,$Hz, corresponding to $\Delta E_0 \approx 2\pi \times 280\,$Hz. Owing to the linear relationship between λ and the tilt ΔE at λ_0 (see figure 1), we have to a very good approximation $\Delta E(t) = \Delta E_0 + b \cdot \sin(\omega t)$, where b is the driving amplitude of the bias energy. The tunnel coupling instead depends not linearly on the control at λ_0, but rather in a polynomial fashion. Thus, the general form of the tunnel coupling is

$$\Omega(t) = \Omega_0 + \sum_m \Omega_1^{(m)} \sin(\mathrm{i}m\omega t) \quad (m = 1, 2, 3, \ldots). \tag{12}$$

We now decompose the Hamiltonian, equation (5) for $U_0 = 0$, into $H = H_0(t) + H_1(t)$, with

$$H_0(t) = \hbar[n\omega + b\sin(\omega t)]\hat{J}_z, \qquad H_1(t) = \hbar(\Delta E_0 - n\omega)\hat{J}_z - \hbar\Omega(t)\hat{J}_x\,. \tag{13}$$

Hereby, n is an integer corresponding to the order of the resonance. Next, we transform into an interaction picture [37] with respect to $H_0(t)$:

$$H_1^{(I)}(t) = \hbar(\Delta E_0 - n\omega)\hat{J}_z - \hbar\Omega(t)\Bigg[e^{-i[n\omega t - \frac{b}{\omega}\cos(\omega t)]}\sum_k |k\rangle\langle k|\hat{J}_x|k+1\rangle\langle k+1|$$
$$+ e^{i[n\omega t - \frac{b}{\omega}\cos(\omega t)]}\sum_k |k\rangle\langle k|\hat{J}_x|k-1\rangle\langle k-1|\Bigg], \tag{14}$$

where we exploited that $\hat{J}_x$ couples $|k\rangle$ only to neighboring states $|k \pm 1\rangle$. Then we insert the generating function of the ordinary Bessel functions $J_l(z)$

$$\mathrm{e}^{\mathrm{i}z\cos(\omega t)} = \sum_{l=-\infty}^{\infty} (\mathrm{i}\,\mathrm{e}^{\mathrm{i}\omega t})^l J_l(z), \tag{15}$$

and obtain

$$H_1^{(\mathrm{I})} = -\hbar\Omega_n^{\mathrm{eff}}\hat{J}_{\phi_n} + \hbar(\Delta E_0 - n\omega)\hat{J}_z, \tag{16}$$

with an effective tunnel coupling Ω_n^{eff},

$$\Omega_n^{\mathrm{eff}} \approx \sqrt{\Omega_0^2 J_n^2 + \sum_{m=1}^{\infty}\left[\Omega_1^{(m)}/2\right]^2 J_{n-m}^2 + \Omega_0 J_n \sum_{k=0}^{\infty}(-1)^k \Omega_1^{(2k+1)} J_{n-2k-1}}, \tag{17}$$

where we omitted the argument in $J_l\left(\frac{b}{\omega}\right)$. Thus, the contributions to the effective tunnel coupling Ω_n^{eff} add up quadratically. Further, we have $\hat{J}_{\phi_n} = \cos(\phi_n)\hat{J}_x + \sin(\phi_n)\hat{J}_y$. The phase ϕ_n has no

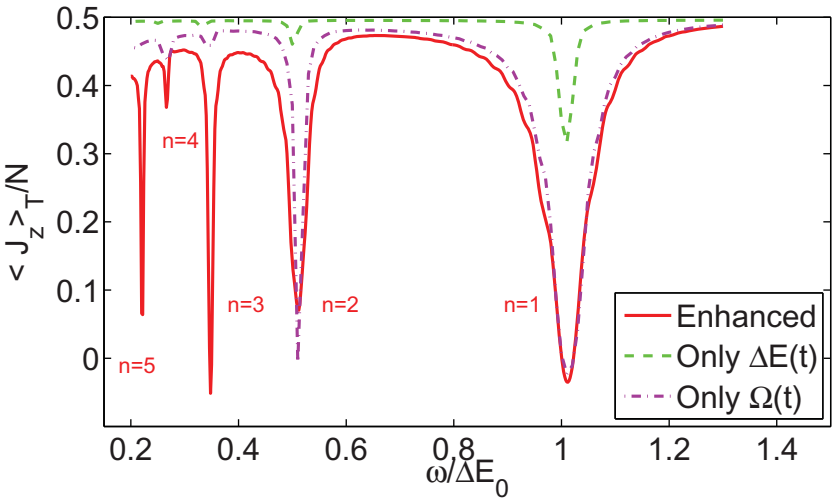

Figure 2. Shapiro resonances for the non-interacting case. The time-averaged population imbalance $\langle \hat{J}_z \rangle_T$ is plotted, with $\omega_0 T = 100$. The driving amplitude λ_1 depends nonlinearly on the driving frequency ω as $\lambda_1 = 0.03 \cdot \Delta E_0/\omega$. Solid line: enhanced Shapiro resonances. Dashed line: the standard Shapiro effect (oscillating $\Delta E(t)$, but constant Ω). Dashed-dotted line: oscillating $\Omega(t)$, but constant ΔE.

influence on the considered Shapiro dynamics of $\langle \hat{J}_z(t) \rangle$, when initially all atoms are in the lower well.

In deriving equation (17) we have neglected fast oscillating terms and kept only the dc contribution, which is reasonable when the frequency is close to the resonance $\omega \approx \Delta E_0/n$ and when it is much larger than the coupling Ω_0 [38, 39]. Furthermore, we have neglected small terms proportional to J_{n+m}.

Thus, the driven system can be approximately described as an undriven system, but with renormalized tunnel coupling [2, 38, 40]. At the resonance condition $n\omega = \Delta E$, there is no effective energy bias between the left and the right condensate, and thus the atoms tunnel at the rate Ω_n^{eff} ('Shapiro current'). For example, the case $n = 0$ corresponds to the trivial resonance of an unbiased system ($\Delta E_0 = 0$) at $\omega = 0$, with Lorentzian line shape characterized by Ω_0^{eff}. The effect of the driving is then to modify the depth and width of the Lorentzian [40]. A system with finite energy bias ($\Delta E_0 \neq 0$) has similar Lorentzian-shaped resonances, but at discrete frequencies $\omega = \Delta E_0/n$.

Most important is the oscillatory part of $\Omega(t)$, which results in additional cross-contributions to Ω_n^{eff}, proportional to $J_{n-m}\left(\frac{b}{\omega}\right)$. Since $J_n(x) > J_{n+1}(x)$ for small values of x, those additional contributions to Ω^{eff} can be considerably larger than those due to the first term under the square root in equation (17), proportional to $J_n\left(\frac{b}{\omega}\right)$. These contributions can drastically enhance the width and depth of the resonances.

A typical resonance structure is reported in figure 2 (solid line), showing distinct resonances up to order $n = 5$.

We have chosen a driving amplitude which increases with the order of the resonance as $\lambda_1 = 0.03 \cdot \Delta E_0/\omega$, such that higher resonances become more distinct. The $n = 1$ resonance

has contributions not only from $J_1\left(\frac{b}{\omega}\right)$, but also from $J_0\left(\frac{b}{\omega}\right)$ since $\Omega_1^{(1)} \neq 0$. The $n = 2$ resonance has contributions not only from $J_2\left(\frac{b}{\omega}\right)$, but also from $J_1\left(\frac{b}{\omega}\right)$ since $\Omega_1^{(1)} \neq 0$ and from $J_0\left(\frac{b}{\omega}\right)$ since $\Omega_1^{(2)} \neq 0$. Because $\Omega_1^{(m)}$ is small when $m > 2$, the width and depth of the resonances become smaller for higher n.

In this figure, we also compare with the case of an artificially constant $\Omega(t)$ ($\Omega_1^{(m)} = 0$ for $m = 1, 2, 3, \ldots$) (dashed line), which shows only extremely weak resonances for $n > 1$ and the same driving amplitude. This is because the effective tunnel coupling Ω^{eff} is proportional to the nth Bessel function $J_n\left(\frac{b}{\omega}\right)$, and our driving amplitude is relatively small, since typically $b \sim n/10$. Thus, the contribution of Bessel functions with $n > 1$ is very small.

In the case of an artificially constant $\Delta E(t)$ ($b = 0$) (dashed-dotted line), we find very pronounced $n = 1$ and $n = 2$ resonances. These resonances are 'trivial' in the sense that they are due to a direct cancellation of the oscillatory terms in equation (14). The strength of the nth resonance thus corresponds to the magnitude of $\Omega_1^{(m)}$, which is largest for $m = 1$ and $m = 2$.

Hence, the combined driving with $\Delta E(t)$ and $\Omega(t)$ yields more than the sum of driving with only one of them, and we thus term these resonances *enhanced Shapiro resonances*. This feature will appreciably facilitate the experimental realization of Shapiro resonances in atomchip-based bosonic Josephson junctions.

3.2. Optimal choice of parameters

We briefly discuss the regime of parameters that are best suited to find clear Shapiro resonances, taking into account the limitations imposed by an experimental realization.

3.2.1. Tunnel coupling Ω. The tunnel coupling Ω, which is determined by the mean double-well separation, controls how fast the atoms tunnel. Therefore, it should be large enough in order that the averaging period for equation (10) is not too long (typically $\omega_0 \Omega T = 15$). If Ω is too large, the resonances are shifted according to $\Delta E \to \sqrt{\Delta E^2 + \Omega^2}$ [2]. Due to the larger-amplitude Rabi oscillations, the resonances get wider and less clear. Another disadvantage of too large Ω is that for an interacting system, the initial state will not be localized [41]. This could be compensated for by choosing a larger tilt, which has however other disadvantages as discussed below.

3.2.2. Asymmetry. Too small an asymmetry (linear gradient g) is unfavorable in experimental realizations as it leads to tunneling dynamics already during the system preparation. Furthermore, the initial state is not well localized, and no clear resonances can be identified when averaging over time. A too large asymmetry, in contrast, requires large driving amplitudes in order to induce a Josephson current.

3.2.3. Driving amplitude b. We have already seen in section 3 that a too small driving amplitude reduces the Shapiro current due to the Bessel function structure. A too large b, however, has the effect of broadening the resonances [$\sim J_n(b/\omega)$].

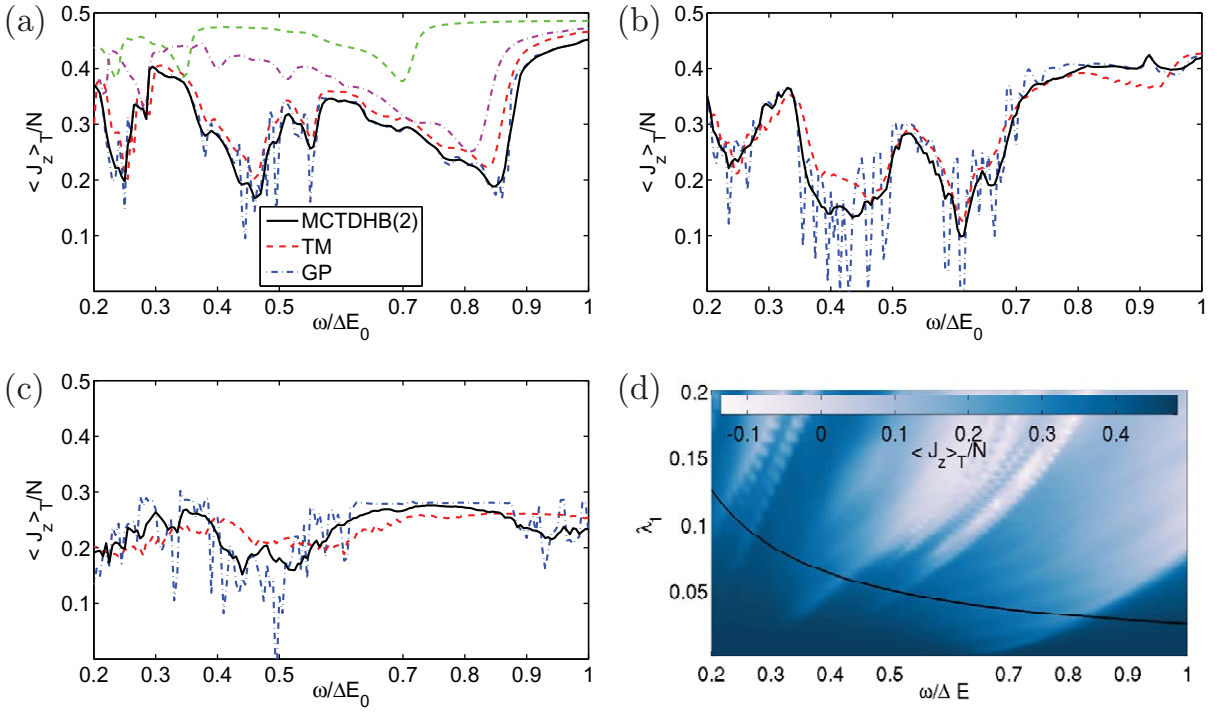

Figure 3. Shapiro resonances for interaction strengths (a–d) $U_0N = \omega_0$, (b) $U_0N = 2\omega_0$ and (c) $U_0N = 4\omega_0$ ($N = 100$). We compare MCTDHB, GP and TM models. For the chosen parameters the GP results show a very strong variation with respect to the driving frequency, in contrast to the TM and MCTDHB results. (a) We also show the case of constant Ω or constant ΔE, similarly to figure 2. $\lambda_1 = 0.035 \cdot \Delta E_0/\omega$ is used. (b) $\lambda_1 = 0.03 \cdot \Delta E_0/\omega$ is used. (c) $\lambda_1 = 0.025 \cdot \Delta E_0/\omega$ is used. (d) Scan over various λ_1 for $U_0N = \omega_0$. The black line corresponds to $\lambda_1 = 0.035 \cdot \Delta E_0/\omega$. Averaging time is $\omega_0 T = 50$.

4. Shapiro resonances in the presence of interactions

4.1. Resonance shifts

Shapiro resonances in a many-body system are shifted in frequency due to atom–atom interactions. For weak interactions, as in [2], the shift is roughly determined by the interaction energy U_0N, with the exact resonance frequencies given in terms of elliptic functions [2, 6]. However, for typical experimental interaction strengths $U_0N \gtrsim \omega_0$ ($\omega_0 = 1/(1.37\,\text{ms})$ is the frequency of a harmonic oscillator with oscillator length $a_0 = \sqrt{\hbar/(m\omega_0)} = 1\,\mu\text{m}$) as we consider here, the resonance frequency itself depends on the driving amplitude λ_1 [40, 42].

The shift in resonances due to interactions is demonstrated using MCTDHB calculations (solid lines in figures 3(a)–(c)), where $\langle \hat{J}_z \rangle_T$ is shown for several interaction strengths, $U_0N = \omega_0$, $U_0N = 2\omega_0$ and $U_0N = 4\omega_0$, respectively.

With increasing interaction strength, the resonances become shifted towards each other. For relatively strong interactions $U_0N = 4\omega_0$ (figure 3(c)), the initial state is not completely localized and the contrast of the resonances is reduced.

The dependence of the resonance shift on the amplitude λ_1 is shown in figure 3(d) for $U_0N = \omega_0$, calculated from the TM model. The shift relative to the $U_0 = 0$ resonances becomes smaller for larger λ_1. The black line corresponds to $\lambda_1 = 0.035 \cdot \Delta E_0/\omega$, which was used in figure 3(a) to map out the resonance most clearly.

For $U_0N = \omega_0$ and for the TM model, we compare also to the case of artificially driving only with $\Omega(t)$ or $\Delta E(t)$, similarly to figure 2. We find that the *enhanced Shapiro resonances* are much more distinct than the usual Shapiro resonances, and the difference is much larger than in the non-interacting case. We also find that the resonance shifts of the usual Shapiro resonances (i.e. at constant Ω) are different from those of the enhanced Shapiro resonances and the case of constant ΔE. This is similar to the findings in [42], where it has been shown that an oscillating $\Omega(t)$ leads to a shift in effective interaction strength.

4.2. Spatial dynamics and damping

Finally, we discuss the limitations of simpler models in describing the driven system. A numerically exact description is provided by the MCTDHB method, such that the MCTDHB results in figures 3(a)–(c) (solid lines) serve as a reference.[8]

We show, in figures 4(b) and (c), example trajectories for the first resonances of (b) $U_0N = \omega_0$, (c) $U_0N = 2\omega_0$ and (d) $U_0N = 4\omega_0$, with the same color code as in figure 3.

The upper panels show the atom number imbalance $\langle \hat{J}_z(t) \rangle$, whereas the middle panels show the time-averaged atom number imbalance $\langle \hat{J}_z \rangle_t = \frac{1}{t} \int_0^t \mathrm{d}t' \langle \hat{J}_z(t') \rangle$.

Both TM- and MCTDHB-based trajectories show damped oscillations, where the decay is faster for stronger interaction strengths. Owing to the nonlinear interactions the BECs become fragmented into two incoherent ($\langle \hat{a}_1^\dagger \hat{a}_2 \rangle = 0$) condensates. In the lower panels of figure 4, we plot the population difference of the natural orbitals $\phi_i(x)$ ($i = 1, 2$) of MCTDHB as a measure of the fragmentation, which leads to a decrease in phase coherence between the left and the right condensate. This is also nicely demonstrated by the width of the number distribution $\Delta J_z(t)$, shown in the upper panels of figures 4(b) and (c) by the bright bands around the mean value (for MCTDHB). Whereas for short times the number distribution is very narrow, it starts to become much broader after a time which depends on the size of the interactions. At the same time, the results from the GP equation, which generally assumes perfect phase coherence for all times, start to deviate from the exact ones. Whereas for MCTDHB and the TM model the width $\Delta J_z(t)$ stays very large and the mean value $\langle \hat{J}_z(t) \rangle$ constant, the GP equation predicts oscillations of $\langle \hat{J}_z(t) \rangle$ with approximately constant amplitude.[9]

In order to point out the importance of renormalizing the tunnel coupling in the TM model according to the last term in equation (7), we also indicate results where it is not included (bright dashed line in figure 4(c)). Fragmentation is clearly important also for larger numbers of atoms, as shown in figure 4(d) for $N = 1000$ atoms (thin line with symbols).[10]

We now turn to the comparison of the resonance curves for different models in figure 3. The driving frequency is much smaller than the transverse trap frequency $\Delta E_0 \ll \omega_{x,y}$, and thus the spatial dynamics of the condensates as shown in figure 4(a) is adiabatic to some extent. Thus, for

[8] We simulated MCTDHB with four orbitals [43, 44] and found that two orbitals allow for a very good description of the physics discussed in this work.

[9] Because of the non-trivial damping dynamics, the time-averaged imbalance $\langle \hat{J}_z \rangle_T$ does not fully characterize the system dynamics, and it is more appropriate to study the full-time evolution of the imbalance.

[10] The interaction strengths considered in this work are typically realized with $N = 100$–1000 atoms.

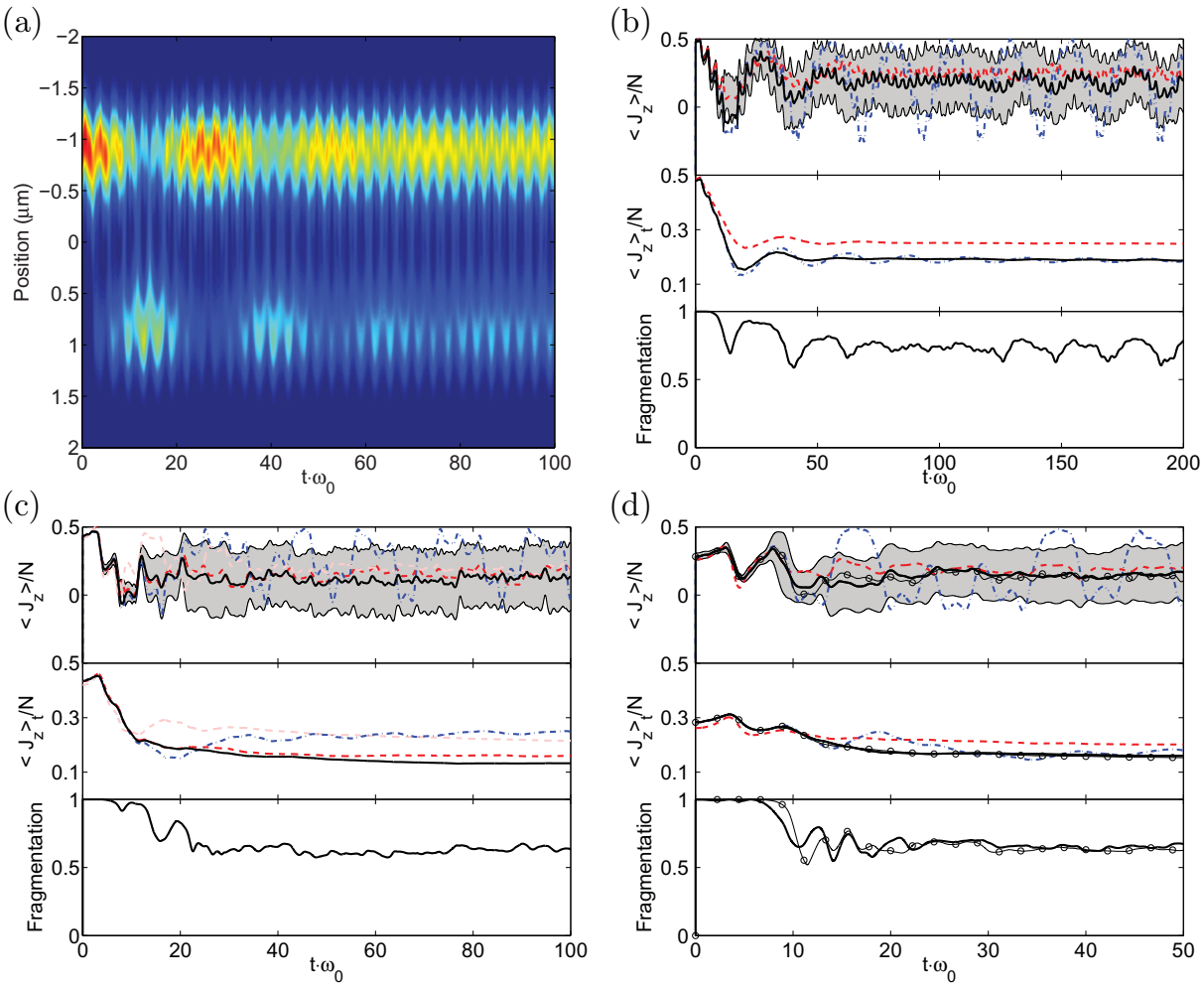

Figure 4. (a) Density for $U_0N = \omega_0$ and driving frequency $\omega/\Delta E_0 = 0.85$. ($N = 100$.) (b–d) Example trajectories for different interaction strengths ($N = 100$), with color code as in figure 3. The upper panel represents $\langle \hat{J}_z(t) \rangle$, where the gray band represents the variance ΔJ_z for MCTDHB, the middle panel the averaged quantity $\langle \hat{J}_z \rangle_t$ and the lower panel the fragmentation $(\rho_{11} - \rho_{22})/N$. (b) $U_0N = \omega_0$ and $\omega/\Delta E_0 = 0.85$. (c) $U_0N = 2\omega_0$ and $\omega/\Delta E_0 = 0.6$. (c) $U_0N = 4\omega_0$ and $\omega/\Delta E_0 = 0.52$. The gray line represents an MCTDHB solution for $N = 1000$ (with U_0N constant).

weak interactions, qualitative agreement between the TM model and MCTDHB can be found. For larger interactions $U_0N = 4\omega_0$, however, they strongly deviate. From this, we conclude that a full self-consistent treatment of the dynamics using MCTDHB becomes necessary. The GP results (dashed-dotted line) are similar to MCTDHB only for the first resonance and $U_0N = \omega_0$. Accordingly, the GP trajectory shows a regular oscillation, a case that has been typically found for the standard Shapiro effect [2]. Generally, however, the GP results (dashed-dotted line) show very fast variations even for small driving frequency variations. This is because trajectories for a slightly different driving frequency deviate strongly after some time. For MCTDHB such deviations are not relevant because of the damping, and thus the curves are much smoother.

5. Conclusion

In conclusion, we have studied Shapiro resonances in a configuration where not only the bias potential, but also the tunnel coupling is driven dynamically. This is typical of double-well potentials realized on atomchips, and thus our findings are directly relevant to future experiments. We show that this configuration has favorable properties as it leads to *enhanced Shapiro resonances*. Owing to a spatial deformation of the potential induced by the driving, the question of transverse excitations is of great interest. We find that, at least for significant interactions, the realistic MCTDHB method has to be used instead of simpler models to properly predict the resonance structure.

Acknowledgments

Special thanks go to Axel U J Lode for explanations and help regarding the MCTDHB package. We thank Alexej I Streltsov, Ofir E Alon, Lorenz S Cederbaum, Aurélien Perrin and Tarik Berrada for most helpful discussions. This work was supported in part by NAWI GASS and the ESF Euroscores program: the EuroQUASAR project QuDeGPM. We also acknowledge support from the Austrian Science Fund within projects P21080-N16, P22590-N16 and F41, by the EU project MIDAS and by the Viennese Fund for Science and Technology (WWTF) projects MA45 and MA07-7. JG acknowledges support from the Alexander von Humboldt Foundation.

References

[1] Barone A and Paterno G 1982 *Physics and Application of the Josephson Effect* (New York: Wiley)
[2] Eckardt A, Jinasundra T, Weiss C and Holthaus M 2005 *Phys. Rev. Lett.* **95** 200401
[3] Tinkham M 1997 *Introduction to Superconductivity* 2nd edn (New York: McGraw-Hill)
[4] Kohler S and Sols F 2003 *New J. Phys.* **5** 94
[5] Baumgärtner F, Sewell R, Eriksson S, Llorente-Garcia I, Dingjan J, Cotter J and Hinds E 2010 *Phys. Rev. Lett.* **105** 243003
[6] Raghavan S, Smerzi A, Fantoni S and Shenoy S R 1999 *Phys. Rev.* A **59** 620
[7] Knoop S, Schuster T, Scelle R, Trautmann A, Appmeier J, Oberthaler M K, Tiesinga E and Tiemann E 2011 *Phys. Rev.* A **83** 042704
[8] Giovanazzi S, Smerzi A and Fantoni S 2000 *Phys. Rev. Lett.* **84** 4521
[9] Zibold T, Nicklas E, Gross C and Oberthaler M K 2010 *Phys. Rev. Lett.* **105** 204101
[10] Morsch O and Oberthaler M 2006 *Rev. Mod. Phys.* **78** 179
[11] Albiez M, Gati R, Folling J, Hunsmann S, Cristiani M and Oberthaler M K 2005 *Phys. Rev. Lett.* **95** 010402
[12] Estève J, Gross C, Weller A, Giovanazzi S and Oberthaler M K 2008 *Nature* **455** 1216
[13] Cataliotti F S, Burger S, Fort C, Maddaloni P, Minardi F, Trombettoni A, Smerzi A and Inguscio M 2001 *Science* **293** 843
[14] Lignier H, Sias C, Ciampini D, Singh Y, Zenesini A, Morsch O and Arimondo E 2007 *Phys. Rev. Lett.* **99** 220403
[15] Zenesini A, Lignier H, Ciampini D, Morsch O and Arimondo E 2009 *Phys. Rev. Lett.* **102** 100403
[16] Eckardt A, Holthaus M, Lignier H, Zenesini A, Ciampini D, Morsch O and Arimondo E 2009 *Phys. Rev.* A **79** 013611
[17] Betz T *et al* 2011 *Phys. Rev. Lett.* **106** 020407
[18] Dalfovo F, Giorgini S, Pitaevskii L P and Stringari S 1999 *Rev. Mod. Phys.* **71** 463
[19] Alon O E, Streltsov A I and Cederbaum L S 2008 *Phys. Rev.* A **77** 033613

[20] Meyer H-D, Gatti F and Worth G A (ed) 2009 *Multidimensional Quantum Dynamics: MCTDH Theory and Applications* (Weinheim: Wiley)
[21] Streltsov A I, Alon O E and Cederbaum L S 2007 *Phys. Rev. Lett.* **99** 030402
[22] Sakmann K, Streltsov A I, Alon O E and Cederbaum L S 2009 *Phys. Rev. Lett.* **103** 220601
[23] Streltsov A I, Alon O E and Cederbaum L S 2011 *Phys. Rev. Lett.* **106** 240401
[24] Sakmann K, Streltsov A I, Alon O E and Cederbaum L S 2010 *Phys. Rev.* A **82** 013620
[25] Schumm T, Hofferberth S, Andersson L M, Wildermuth S, Groth S, Bar-Joseph I, Schmiedmayer J and Krüger P 2005 *Nature Phys.* **1** 57
[26] Lesanovsky I, Schumm T, Hofferberth S, Andersson L M, Krüger P and Schmiedmayer J 2006 *Phys. Rev.* A **73** 033619
[27] Hofferberth S, Fischer B, Schumm T, Schmiedmayer J and Lesanovsky I 2007 *Phys. Rev.* A **76** 013401
[28] Krüger P, Luo X, Klein M W, Brugger K, Haase A, Wildermuth S, Groth S, Bar-Joseph I, Folman R and Schmiedmayer J 2003 *Phys. Rev. Lett.* **91** 233201
[29] LeBlanc L J, Bardon A B, McKeever J, Extavour M H T, Jervis D, Thywissen J H, Piazza F and Smerzi A 2011 *Phys. Rev. Lett.* **106** 025302
[30] Leggett A 2001 *Rev. Mod. Phys.* **73** 307
[31] Grond J, von Winckel G, Schmiedmayer J and Hohenester U 2009 *Phys. Rev.* A **80** 053625
[32] Pitaevskii L and Stringari S 2001 *Phys. Rev. Lett.* **87** 180402
[33] Javanainen J and Ivanov M Y 1999 *Phys. Rev.* A **60** 2351
[34] Ananikian D and Bergeman T 2006 *Phys. Rev.* A **73** 013604
[35] Sakmann K, Streltsov A I, Alon O E and Cederbaum L S 2008 *Phys. Rev.* A **78** 023615
[36] Penrose O and Onsager L 1956 *Phys. Rev.* **104** 576
[37] Sakurai J J 1994 *Modern Quantum Mechanics* (Reading, MA: Addison-Wesley)
[38] Jinasundera T, Weiss C and Holthaus M 2006 *Chem. Phys.* **322** 118
[39] Grifoni M and Hänggi P 1998 *Phys. Rep.* **304** 229
[40] Tsukada N, Gotoda M, Nomura Y and Isu T 1999 *Phys. Rev.* A **59** 3862
[41] Streltsov A I, Alon O E and Cederbaum L S 2006 *Phys. Rev.* A **73** 063626
[42] Zhang Q, Hänggi P and Gong J 2008 *Phys. Rev.* A **77** 053607
[43] Streltsov A I, Sakmann K, Lode A U J, Alon O E and Cederbaum L S 2010 *The Multiconfigurational Time-Dependent Hartree for Bosons Package, Version 2.0* (Heidelberg: Springer) http://mctdhb.uni-hd.de
[44] Streltsov A I, Alon O E and Cederbaum L S 2010 *Phys. Rev.* A **81** 022124